Fullerenes, Nanotubes, and Carbon Nanostructures, 13: 299–311, 2005

ISSN 1536-383X print/1536-4046 online
DOI: 10.1080/15363830500237143

Taylor & Francis
Taylor & Francis Group

Anisotropies in Carbon Nanotube Synthesis by the Hydrogen Arc Plasma Jet Method

V. Cruz-Alvarez, J. Ortiz-López, and C. Mejía-García
Instituto Politécnico Nacional, Escuela Superior de Física y Matemáticas, U.P.A.L.M. de Zacatenco, Mexico

J. S. Arellano-Peraza and V. M. Sánchez-Martínez
Universidad Autónoma Metropolitana Azcapotzalco, Mexico

J. Chávez-Carvayar
Instituto de Investigaciones en Materiales—U.N.A.M., Mexico

Abstract: Single-wall carbon nanotubes were prepared under hydrogen gas atmosphere with a DC arc discharge maintained between the tip of a sharpened graphite cathode and an anode formed by a catalytic mixture of graphite, FeS, Ni, Fe and Co compressed powders. The cathode is placed with an inclination with respect to the anode, so that the plasma jet of the discharge is deviated towards the empty space of the growth chamber. Samples were classified and analyzed according to their type and growth positions relative to the direction of the plasma jet flow. Characterization of the samples was performed with mass spectrometry, Raman spectroscopy and transmission electron microscopy. A subtle variation is found in the properties of the nanotubes obtained in different locations due to the directionality of the plasma jet flow. Observed differences in sample properties may be qualitatively understood in terms of accepted mechanisms of SWNT growth.

Keywords: Carbon nanotubes, electric arc discharge, Raman scattering

Received 12 April 2005, Accepted 16 April 2005
Address correspondence to Dr. Jaime Ortiz-López, Instituto Politécnico Nacional, Escuela Superior de Física y Matemáticas, U.P.A.L.M. de Zacatenco, Edificio 9, 07738, Mexico D.F., Mexico. E-mail: jortiz@esfm.ipn.mx

INTRODUCTION

Single-wall carbon nanotubes (SWNT) are unique nanostructured materials composed of only one rolled graphene sheet (1). Bulk quantities of these materials are promising candidates for gas storage applications (2). Three conventional methods for mass-production of single-wall carbon nanotubes (SWNT) have been developed over the years: laser ablation (3), chemical vapour deposition (4), and arc discharge (5) techniques. Among these, the last two are low cost and easy to implement. In the typical arc discharge method (5), a high DC electric current is established in an inert gas atmosphere between a carbon cathode and a metal-doped carbon rod (anode) placed in front of each other with a small separation distance. SWNTs produced with this technique are found in bundles in a collar deposit around the anode. The so-called "arc plasma jet method" is a variation of the conventional arc discharge technique in which the electrodes are placed with a relative inclination between each other so that a plasma jet is formed during the arc discharge (6, 7). This electrode arrangement allows the production of free-standing macroscopically long ropes (up to 100 mm in length) of aligned SWNTs (6) and increases the yield of cotton-like carbon soot containing SWNTs (7). Since the plasma jet is highly directional, differences in the quality and characteristics of the produced SWNTs at different positions in the growth chamber are expected to occur. To the best of our knowledge, experimental corroboration of this assertion has never been undertaken before.

In this work we use the arc plasma jet technique to synthesize SWNTs under hydrogen atmosphere to carefully analyze samples obtained in five different locations of the growth chamber. Our analyses demonstrate that this method of SWNT synthesis is indeed anisotropic so that the characteristics of the obtained samples depend on their growth positions relative to the plasma jet direction. The samples studied were non-purified "as grown" raw samples to avoid perturbation of their site-dependent properties. Usual purification methods (acid washing, oxidation, etc.) can modify or even destroy some nanotubes and could be detrimental in the detection of subtle differences between raw samples obtained at different sites. Characterization of the samples was performed with mass spectrometry, Raman spectroscopy, and transmission electron microscopy.

EXPERIMENTAL DETAILS

Carbon nanotubes were prepared under hydrogen gas atmosphere (200 torr) by a modified arc-discharge technique similar to the one described by Liu et al. (6). In our case, a DC current of about 150 A is provided by a 22.8 kVA commercial arc welding equipment externally connected to a bell jar evaporator, which is used as a growth chamber. The discharge is maintained between the tip of a sharpened graphite cathode and an anode formed

by a catalytic mixture of powders with (molar) composition 95% C (graphite), 1% FeS and 4% of a Ni : Fe : Co mixture in the proportion 5 : 1 : 1 atomic. These powders are compressed inside cavities carved on a supporting graphite block. The cathode is placed with an inclination of about 60° above the filled cavities so that the plasma jet of the discharge is deviated towards the empty volume of the growth chamber. The cathode support is designed to have rotational motion about a vertical axis allowing the cathode tip to be swept along several filled cavities. In this way, a considerable amount of catalytic mixture can be consumed in a single run. The amount of raw material collected after 6 runs was close to 16 grams. The use of H_2 gas has the advantage of being more effective in quenching the plasma flow and keeps the surface of catalytic particles free of oxides or carbon (6). The addition of a sulphur-containing substance such as FeS promotes the growth of nanotubes under H_2 atmosphere (6).

After the discharge is triggered, a black web-like material grows and hangs from objects and supports inside the chamber and, at the same time a fluffy black film is deposited on the chamber walls. The obtained samples were classified according to their type and growth positions relative to the direction of the plasma jet and labelled as follows: "web" (W), "front" (F), "side" (S), "top" (T), and "behind" (B). These sites are defined in the schematic illustration shown in Figure 1. Distances from the plasma

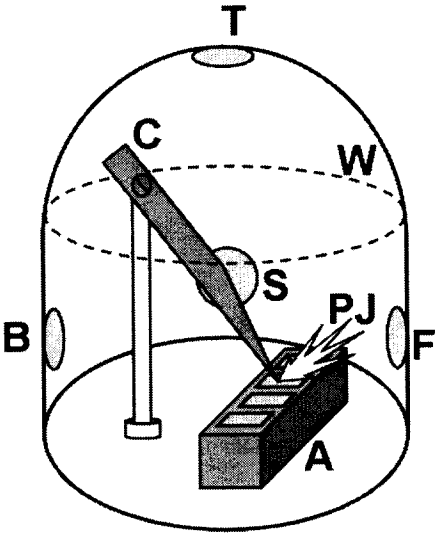

Figure 1. Schematic illustration of the arc discharge chamber. C, sharpened graphite cathode with $\sim 60°$ inclination; A, graphite anode block with cavities filled with catalytic mixture; PJ, plasma jet. Selected sites from where samples were extracted: F, front; S, side; T, top; B, back. The web-like material was caught by a wire grid (not drawn) placed horizontally about the dashed line denoted by W.

jet to these sites were 15 cm for W, F, S and B, and 30 cm for T. The plasma jet was of average elongated shape with about 1.5 cm length.

To detect the relative amount of catalytic residues in the samples, mass spectra was obtained with a time-of-flight mass spectrometer (Comstock R-1M) operated in the reflectron mode with a 10 kV accelerating voltage to detect positive ions. Samples for mass spectra were collected on thin aluminium plates located at strategic positions inside the growth chamber. These plates were then mounted on the instrument sample holder for analysis. Non-polarized micro-Raman analysis of the samples with $2\,cm^{-1}$ spectral resolution was performed with $\lambda = 514.5$ nm excitation ($E_{laser} = 2.41$ eV) from an argon ion laser in conjunction with a CCD camera for detection. Samples for Raman spectroscopy were collected from walls and hanging material inside the growth chamber, placed on microscope slides and then mounted on a microscope with a 100x objective lens. Transmission electron microscopy (TEM) was performed with a JEOL-2010 instrument operated at 120 kV. In this case, samples collected from the chamber were sonicated in ethanol for 30 minutes and then deposited by dripping on TEM copper grids.

RESULTS

A typical transmission electron microscopy (TEM) image of sample "top" (T) is presented in Figure 2. Images of other samples show the same general appearance. Across this image, in a diagonal direction from lower left to

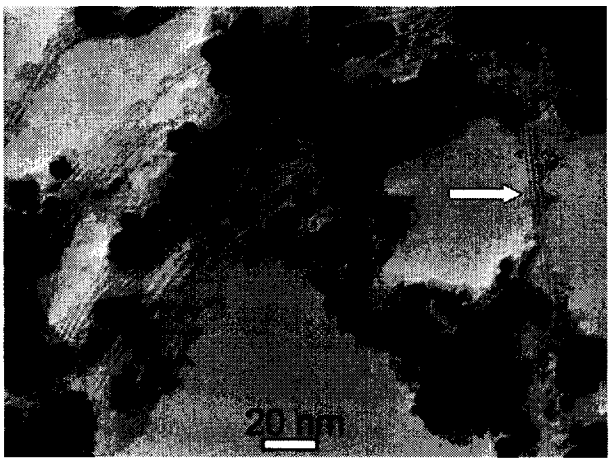

Figure 2. Typical transmission electron microscopy image of sample "top" (T). Images of other samples have the same general appearance. The arrow points to a couple of entangled SWNTs of about 2 nm diameter.

upper right, we can see a bundle of SWNTs bonded together with catalyst particles through a sort of membrane, perhaps amorphous carbon, which shows no evident structure. The arrow shown points to a couple of entangled SWNTs with diameters of about 2 nm.

The observed residues of metal catalysts were detected and analyzed with mass spectrometry. The inset in Figure 3 shows a typical spectrum for sample "front" (F) in which Ni, Fe, and Co isotopic peaks are clearly seen corroborating the presence of catalytic residues in the synthesized material. By carefully taking the spectra of all samples under same conditions it is possible to directly compare the intensity of the peaks to determine the relative content of catalytic metals for each sample. In Figure 3 we show a bar diagram of the relative intensities of ^{58}Ni, ^{56}Fe, and ^{59}Co peaks for each sample. All intensities are roughly the same except for that of sample F (front), which is about five times larger as the other ones. Therefore, sample F has five times more catalytic mixture than any of the other ones.

Figures 4a and 4b show Raman spectra taken in region D (1200–1400 cm^{-1}) and region G (1500–1700 cm^{-1}), respectively. Note the different scales for each spectrum. The band observed in region D for all samples

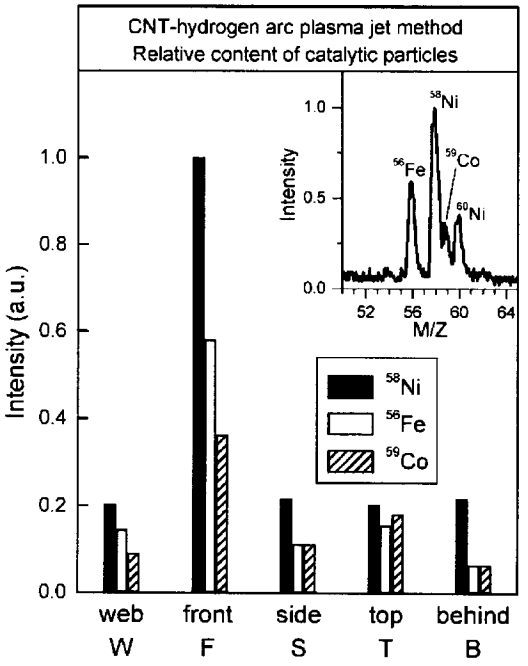

Figure 3. Comparison of ^{58}Ni, ^{56}Fe, and ^{59}Co relative peak intensities in mass spectra of the five types of studied samples. The inset shows a typical spectra in the case of sample collected in front of the plasma jet (sample "front", F).

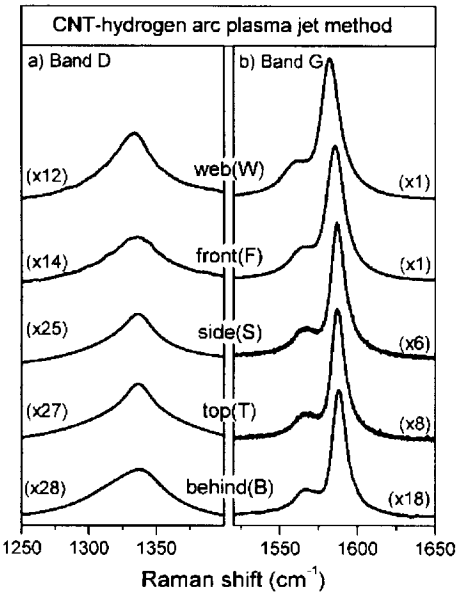

Figure 4. Raman spectra of all samples; a) for region D, and b) for region G. Note the different scales for each spectrum.

indicates the presence of structural defects associated with carbonaceous material in our samples, including possibly the occurrence of amorphous carbon, graphitic particles or defective carbon nanotubes (single- or multiple-walled). The split line shape of the G-band is unmistakable evidence of the existence of SWNTs in all samples. The response in both D and G regions for the different samples show subtle variations due to anisotropic conditions of SWNT synthesis as we discuss in the next section.

DISCUSSION

Direct TEM observation of our samples indicates that they consist of SWNT bundles, catalyst particles and amorphous carbon. The circumstance that sample "front" (F) contains five times more catalytic residues than the other ones reflects, of course, the fact that the plasma jet drags the catalytic mixture along with it, and already represents an indication of anisotropic conditions in SWNT synthesis with the arc plasma jet method.

Raman scattering in SWNTs is a resonant process associated with allowed optical transitions between van Hove singularities in their 1-D electronic density of states that fall in the visible and infrared range. Raman spectroscopy allows meticulous characterization of SWNTs by looking at the response in three spectral regions denoted as RBM, G and D, corresponding to the

excitation of related SWNT vibrational modes (8). Although Raman spectra in region RBM (radial breathing mode) in the range $120-250\,cm^{-1}$ (for diameters 1–2 nm) provides essential data about the diameter distribution of resonant tubes in a given sample, a great deal of information can also be obtained from G and D modes.

The response displayed in Figure 4b for region G, consisting of a large peak (known as G+) accompanied at low frequency by a smaller one (known as G−) indicates undoubtedly the presence of resonant SWNTs in all of our samples. The pair G+ and G− is due to the splitting of tangential modes parallel and perpendicular to the tube axis, respectively (8). Moreover, the evident symmetric line shape of the G− band indicates additionally that the signal is due to resonant semiconducting nanotubes (8). Given that the excitation energy of our Raman measurement is 2.41 eV, the so-called Kataura plot (9) ascertains that resonant semiconducting SWNTs in our samples should have a diameter distribution in the range $1.3 \leq d_t \leq 2.0$ nm, corresponding to electronic transition energies E_{33}^S and E_{44}^S. Our TEM observations discard the presence of nanotubes with diameters outside this range. Liu et al. (6), using the plasma jet method with Ni/Fe/S catalysts, obtained SWNTs with diameters within this range (1.79 nm).

Lorentzian line shape analysis of the measured G-band is shown in Figure 5. For all samples the response is well described with three

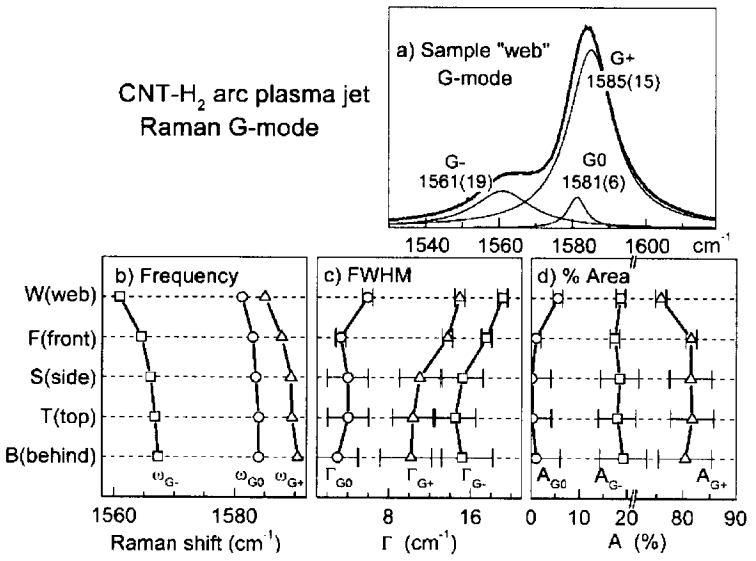

Figure 5. a) Lorentzian line shape analysis of band G for sample "web" showing frequency positions and widths (in parenthesis); b) evolution of Lorentzian peak positions ω_{G-}, ω_{G0}, and ω_{G+} for all studied samples; c) evolution of widths (FWHM) Γ_{G-}, Γ_{G0} and Γ_{G+}; d) evolution of relative integrated intensities A_{G-}, A_{G0}, and A_{G+}.

Lorentzian peaks. For instance, Figure 5a shows the analysis for sample "web" (W). The first Lorentzian G− is located at $\omega_{G-} = 1561\,cm^{-1}$ with a FWHM (full width at half maximum) $\Gamma_{G-} = 19\,cm^{-1}$, the second one G0 is narrower, having $\Gamma_{G0} = 6\,cm^{-1}$ and located at an intermediate frequency $\omega_{G0} = 1581\,cm^{-1}$, and the third one G+ is at a higher frequency $\omega_{G+} = 1585\,cm^{-1}$ with $\Gamma_{G+} = 15\,cm^{-1}$. The same situation is observed for the rest of the samples, that is, the response can always be described by three Lorentzians. The evolution of their frequency positions ω_{G-}, ω_{G0}, ω_{G+}, their widths Γ_{G-}, Γ_{G0}, Γ_{G+} and their integrated intensities A_{G-}, A_{G0}, A_{G+} for the different samples shows interesting features and variations as can be seen in Figure 5b, 5c, and 5d, respectively. Note that the order in which samples are arranged in these figures was chosen intentionally to reveal a rough trend in the plotted values. Note also that samples S (side) and T (top) should be correlated or alike, since they are formed along equivalent directions with respect to the plasma flow.

The nearly parallel evolution of parameters for these two samples in Figure 5 (as well as in Figure 6) seems to confirm this assertion. The Lorentzian G0 is always the narrowest (Figure 5c), its contribution (that is %A, in Figure 5d) is of 5% in sample W, of 1% for samples F and B and

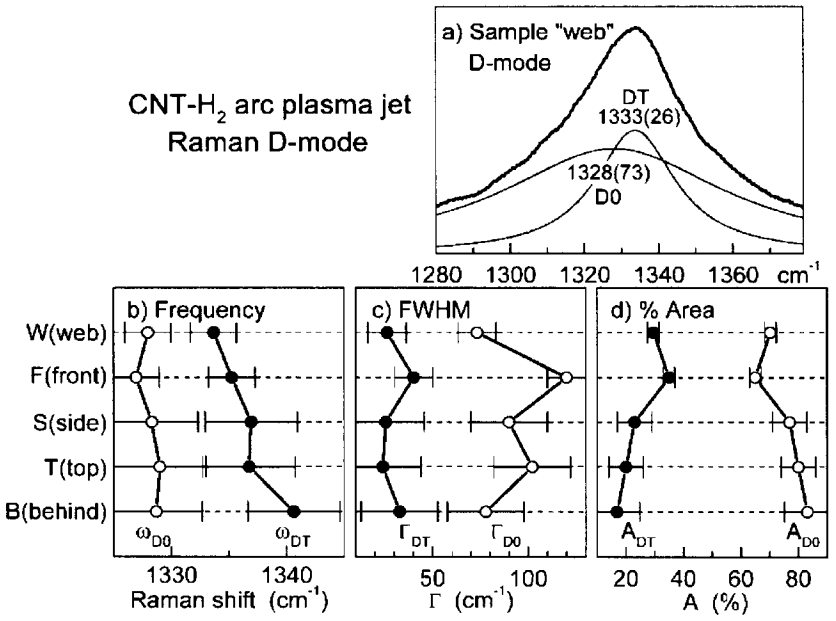

Figure 6. a) Lorentzian line shape analysis of band D for sample "web" (W) showing frequency positions and widths (in parenthesis); b) evolution of Lorentzian peak positions ω_{D0} and ω_{DT} for all studied samples; c) evolution of widths (FWHM) Γ_{D0} and Γ_{DT}; d) evolution of relative integrated intensities A_{D0} and A_{DT}.

negligible for samples S and T. Its frequency position ω_{G0} is nearly the same for all samples (Figure 5b), it is positioned within $1583 \pm 1\,cm^{-1}$, which is close to $1582\,cm^{-1}$, the frequency of the tangential mode in graphite and multi-wall carbon nanotubes (MWNT) (8). Thus, the integrated intensity of Lorentzian G0 can be taken as rough measure of the content of graphitic particles (including metal clusters encapsulated within graphene layers) and MWNTs in our samples, namely, sample W contains five times more of them than samples F and B while samples S and T are free of them. In contrast, for all samples both Lorentzians G− and G+ are significantly wider and participate roughly in the same proportions (20% and 80%, respectively). Their frequency positions show an increasing trend as we go from sample W to sample B (Figure 5b). From group theory, the Raman G-mode in isolated SWNTs is expected to consist of six phonon modes. The intensity with which each mode participates depends on the chirality of the tube so that only three of them are expected for achiral nanotubes (zig-zag or armchair) while all of them should contribute for chiral nanotubes (10).

The G-band line shape of an isolated SWNT therefore depends on the nanotube chiral angle θ. For zig-zag tubes ($\theta = 0°$), the G+ band (at a fixed frequency of $1591\,cm^{-1}$) dominates the spectrum since the G− band is weak. On the contrary, for armchair tubes ($\theta = 30°$, always metallic) the G− band dominates and is located at a frequency that depends on the tube diameter d_t as $\sim 1/d_t^2$. The "typical" G+/G− band pair occurs for chiral semiconducting SWNTs with $0° < \theta < 30°$ with a large G+ and smaller G− bands each positioned as just described. The diameter d_t (in nm) of a SWNT can be estimated with the equation: $d_t = \sqrt{(45.7/\Delta\omega)}$, in which $\Delta\omega = \omega_{G+} - \omega_{G-}$, with $\omega_{G+} = 1591\,cm^{-1}$ (8). As our samples clearly contain a heterogeneous mixture of SWNTs in bundles and ropes with a distribution of tube diameters and chiral angles, their G-band spectrum should consist of an overlap of many peaks from different nanotubes in resonance with the excitation energy (2.41 eV) in our measurements. Hence, G− and G+ modes in our samples result in the inhomogeneously broadened Lorentzian peaks described in Figure 5. As seen in Figure 5b, the frequency position of band G+ is close to $1591\,cm^{-1}$ (as in isolated SWNTs) in the case of samples S, T, and B, while for samples W and F, it is downshifted 6 and $3\,cm^{-1}$, respectively. This downshift could be associated with preferential chirality (θ towards 30°) or with bundle and impurity effects. Exact assessment of these possibilities would require detailed studies such as photoluminescence, which are outside of the scope of the present report. Equation (1) can be applied to our data to estimate an average diameter and distribution width of resonant nanotubes for the different samples as listed in Table 1. As can be seen, the average tube diameter $\bar{d}_t$ in all samples is about the same except for sample W, which is slightly smaller.

The band observed in region D for all samples indicates the presence of amorphous carbon and/or defective nanotubes. It is usual to measure the structural quality of a SWNT sample by the ratio I_G/I_D between the intensities

Table 1. Average nanotube diameters $\bar{d}_t$ and estimated distribution widths Δd of resonant semiconducting SWNTs calculated with equation (1) for the different samples

Sample	$\bar{d}_t \pm \Delta d$ (nm)	I_{G+}/I_D
Web (W)	1.38 ± 0.12	34.05
Front (F)	1.40 ± 0.11	49.25
Side (S)	1.40 ± 0.12	26.50
Top (T)	1.42 ± 0.08	27.02
Behind (B)	1.40 ± 0.15	11.26

Intensity ratios I_{G+}/I_D obtained from the measured G+ and D bands.

of peaks G and D. The larger this ratio, the better the structural quality of the sample. In Table 1 we list this ratio (actually I_{G+}/I_D, where G+ denotes the main peak of the G-band in Figure 5b) for all measured samples. The largest values are obtained for samples W and F while the smallest occurs for sample B. Therefore, best quality samples synthesized by the arc plasma jet method are those obtained as web-like hanging material (W) and as film on the chamber walls in the forward direction of the plasma jet flow (F). The worst case of sample B indicates the augmented formation of amorphous carbon and incomplete growth of nanotubes in the backward direction of the plasma flow.

Line shape analysis of the measured D bands is well described by a superposition of two Lorentzians with subtle differences between samples. As an illustrative example, in Figure 6a we show the deconvolution of band D for sample W. The first Lorentzian D0 is located at $\omega_{D0} = 1328\,cm^{-1}$ with a width $\Gamma_{D0} = 73\,cm^{-1}$ while the second Lorentzian DT is narrower, having $\Gamma_{DT} = 26\,cm^{-1}$ and located at a slightly higher frequency $\omega_{DT} = 1333\,cm^{-1}$. The same situation is observed for the rest of the samples, that is, the response can always be described by a wide Lorentzian at low frequency (D0) and a narrower one at higher frequency (DT). The evolution of frequency positions of both Lorentzians (ω_{D0} and ω_{DT}) with sample type shows subtle variations as can be observed in Figure 6b (the order in which samples are arranged in this figure is the same as in Figure 5). It can be seen that ω_{D0} is nearly the same for all samples while ω_{DT} slightly shifts to lower frequency as we go from samples B to W in Figure 6b. On the other hand, for the evolution of the widths Γ_{D0} and Γ_{DT} in Figure 6c, no special trend can be recognized except for a moderate dispersion of Γ_{DT} around $28\,cm^{-1}$ and an irregular behaviour of Γ_{D0} around a mean value of $90\,cm^{-1}$. It is well known that the D-band in SWNTs samples is composed of a broad peak on top of which is superimposed a sharper peak, the broad feature coming from amorphous carbon and the sharper feature coming from carbon nanotubes (8). Therefore, the D-band

measured in all our samples confirms the presence of both amorphous carbon through the wide Lorentzian D0 and of nanotubes through the narrow Lorentzian DT. The mean value of $28\,cm^{-1}$ for Γ_{DT} in our samples is comparable with values in the range $7-40\,cm^{-1}$ measured in a large variety of isolated SWNTs (11). In the evolution of the integrated intensities A_{DT} and A_{D0} in Figure 6d, it is revealed that for samples W and F the contribution of Lorentzian DT is greatest (30–35%) while in sample B the highest contribution (83%) of Lorentzian D0 occurs. Since DT is associated with defective nanotubes while D0 with amorphous carbon, this gives extra account to the already described condition of sample B as the most defective one (i.e., lowest I_G/I_D ratio).

In SWNTs, the dispersive disorder-induced D-mode is associated with a double resonance process and its frequency, intensity and line width carry important information not only about the degree of disorder but also about compressive or tensile strain. The D-band frequency ω_D has been found to depend in different ways on the tube diameter d_t if the range of diameters present in a given sample of SWNTs is either a wide or a narrow one (12, 13). We have tested for a dependence of ω_{DT} (Figure 6) with d_t (Table 1) in our data but we have not found any. Evidently, the behavior displayed by our samples is much more difficult to describe than in isolated SWNTs due to their heterogeneous nature. We must bear in mind that the D-mode response can also be influenced by the state of mechanical strain. Within our "as grown" raw samples there surely must be lots of bended and deformed SWNTs that certainly affect the response in an unpredictable and complicated way.

The observed properties of our SWNT samples reveal subtle differences that depend on the direction of the plasma jet flow. This is due to the anisotropic shape of the plasma jet whose thickness, length, and shape depend on the cathode/anode angle, the DC arc current and the pressure of the H_2 gas (6, 7). These conditions result in temperatures and temperature gradients in the plasma jet that have highly directional variations. According to proposed mechanisms for SWNT synthesis (14), during the cooling process of the hot plasma formed from the vaporized catalytic mixture, small carbon molecules and atoms condense to form larger clusters. The catalysts condense more slowly and attach to carbon clusters and prevent their closing. From these initial clusters, tubular carbon molecules grow into SWNTs until the catalyst particles become too large, or until conditions have cooled sufficiently that carbon no longer can diffuse through or on the catalyst particles.

A qualitative explanation to our results can be given in terms of the above considerations. In the backward direction there is no plasma jet flow so that SWNTs in sample B (behind) should have arrived after a long flight time. Since the temperature would have already decreased considerably, more carbon atoms and/or clusters may be trapped during flight without contributing to the formation of SWNTs and appear as amorphous carbon at the end. Sample B should then have amorphous carbon or defective SWNTs in

greater proportions. On the other hand, along the forward direction, the temperature gradient should be small and catalysts should be more abundant (due to the dragging effect of the plasma) so that the probability of the formation of high quality SWNT is higher as found in sample F (front). In perpendicular directions of the plasma jet flow, the temperature gradient should be large and catalyst less abundant so that conditions for the growth of good quality SWNTs are less favourable. This corresponds to our samples S (side) and T (top), which as already pointed out and confirmed must be correlated and alike due to their symmetric locations perpendicular to the plasma jet flow. In the case of sample W (web), wandering material with moderate flight times originally coming from several directions of the plasma jet gets deposited with slow arrival speed and hangs from objects inside the chamber. Deposition in this case is more gentle, so that their length and structural integrity is conserved without breaking or bending resulting in long bundles of good quality SWNTs.

SUMMARY

We have used the arc plasma jet technique to synthesize SWNTs with DC arc current under hydrogen atmosphere. Analysis of samples was performed with mass spectrometry, Raman spectroscopy, and transmission electron microscopy. Our analysis demonstrate that this method of synthesis is anisotropic so that the characteristics of the obtained samples depend on their growth positions relative to the plasma jet flow direction. Best quality samples are obtained as film deposits in the forward direction of the plasma jet, and as hanging web-like material. The inherent anisotropy is consequence of the high directionality of the plasma jet. Observed differences in sample properties may be understood in terms of accepted mechanisms of SWNT growth.

ACKNOWLEDGMENTS

One of us (J.O.L.) gratefully acknowledges CGPI-IPN for support to Projects Nos. 20010558 and 20020911, and to COFAA-IPN for a SIBE fellowship.

REFERENCES

1. Iijima, S. and Ichihasi, T. (1993) Single-shell carbon nanotubes of 1-nm diameter. *Nature*, 363: 603–605.
2. Liu, C., Fan, Y.Y., Liu, M., Cong, H.T., Cheng, H.M., and Dresselhaus, M.S. (1999) Hydrogen storage in single-walled carbon nanotubes at room temperature. *Science*, 286: 1127–1129.

3. Thess, A., Lee, R., Nikolaev, T., Dai, H., Petit, P., Robert, J., Xu, C., Lee, Y.H., Kim, S.G., Rinzler, A.G., Colbert, D.T., Scuseria, G.E., Tomanek, D., Fischer, J.E., and Smalley, R.E. (1996) Crystalline ropes of metallic carbon nanotubes. *Science*, 273: 483–487.
4. Endo, M., Takeuchi, K., Igarashi, S., Kobori, K., Shiraishi, M., and Kroto, H.W. (1993) The production and structure of pyrolytic carbon nanotubes (PCNT's). *J. Phys. Chem. Solids*, 54: 1841–1848.
5. Journet, C., Maser, W.K., Bernier, P., Loiseau, A., Lamy de la Chapelle, M., Lefrant, S., Deniard, P., Lee, R., and Fischer, J.E. (1997) Large-scale production of single-walled nanotubes by the electric-arc technique. *Nature*, 388: 756–758.
6. Liu, C., Cong, H.T., Li, F., Tan, P.H., Cheng, H.M., Lu, K., and Zhou, B.L. (1999) Semi-continuous synthesis of single-walled carbon nanotubes by a hydrogen arc discharge method. *Carbon*, 37: 1865–1868, and Liu, C., Cheng, H.M., Cong, H.T., Li, F., Su, G., Zhou, B.L., and Dresselhaus, M.S. (2000) Synthesis of macroscopically long ropes of well-aligned single-walled carbon nanotubes. *Adv. Mater. 12*: 1190–1192.
7. Ando, Y., Zhao, X., Hirahara, K., Suenaga, K., Bandow, S., and Iijima, S. (2000) Mass production of single-wall carbon nanotubes by the arc plasma jet method. *Chem. Phys. Lett.*, 323: 580–585.
8. Jorio, A., Pimenta, M.A., Souza Filho, A.G., Saito, R., Dresselhaus, G., and Dresselhaus, M.S. (2003) Characterizing carbon nanotube samples with resonance Raman scattering. *New J. Phys.*, 5: 139.1–139.17.
9. Kataura, H., Kumazawa, Y., Maniwa, Y., Umezu, I., Susuki, S., Ohtzuka, Y., and Achiba, Y. (1999) Optical properties of single-wall carbon nanotubes. *Synth. Met.*, 103: 2555–2558.
10. Saito, R., Jorio, A., Hafner, H., Lieber, C.M., Hunter, M., McClure, T., Dresselhaus, G., and Dresselhaus, M.S. (2001) Chirality-dependent G-band Raman intensity of carbon nanotubes. *Phys. Rev. B*, 64: 085312.1–085312.7.
11. Jorio, A., Fantini, C., Dantas, M.S.S., Pimenta, M.A., Souza Filho, A.G., Samsonidze, Ge.G., Brar, V.W., Dresselhaus, G., Dresselhaus, M.S., Swan, A.K., Unlü, M.S., Goldberg, B.B., and Saito, R. (2002) Linewidth of the Raman features of individual single-wall carbon nanotubes. *Phys. Rev. B*, 66: 115411.1–115411.8.
12. Souza Filho, A.G., Jorio, A., Samsonidze, Ge.G., Dresselhaus, G., Pimenta, M.A., Dresselhaus, M.S., Swan, A.K., Unlü, M.S., Goldberg, B.B., and Saito, R. (2003) Competing spring constant versus double resonance effects on the properties of dispersive modes in isolated single-wall carbon nanotubes. *Phys. Rev. B*, 67: 035427.1–035427.7.
13. Dresselhaus, M.S., Dresselhaus, G., Jorio, A., Souza Filho, A.G., and Saito, R. (2002) Raman spectroscopy on isolated single wall carbon nanotubes. *Carbon*, 40: 2043–2061.
14. Scott, C.D., Arepalli, S., Nikolaev, P., and Smalley, R.E. (2001) Growth mechanisms for single-wall carbon nanotubes in a laser-ablation process. *Appl. Phys. A*, 72: 573–580.